ISSN 1590-8844
International Journal of Mechanics and Control, Vol. 24, No. 02, 2023

https://doi.org/10.69076/jomac.2024.0020

PRELIMINARY DESIGN OF THE GUIDANCE AND CONTROL SYSTEM OF A LUNAR DRONE

S. Pescaglia*, G. Bortolato*, A. Revello*, P. Maggiore*, R. Vittori**

* Department of Mechanical and Aerospace Engineering, Politecnico di Torino, Italy

** ESA Astronaut, General of Italian Air Force

ABSTRACT

This paper presents the preliminary design of the Guidance and Control System of a lunar nano (LuNaDrone). This small, rocket-propelled spacecraft is equipped with autonomous navigation, which provides the drone with the ability to fly over the lunar surface. The extreme mobility capabilities of this spacecraft allow a wide range of applications, from exploring sites of interest to last-mile delivery of small payloads. One of the most demanding use-case scenarios is the exploration of lunar pits, which are particularly interesting as some of them may provide access to underground lava tubes. This application is the one considered for the preliminary design of LuNaDrone's guidance and control system. The flight profile for this mission is a fixed altitude trajectory that can be subdivided into a sequence of elementary manoeuvres. The guidance algorithm presented in this paper allow for the evaluation of the desired state and ideal controls at each point of the trajectory. The tuning of the controller, a Finite-Horizon Linear Quadratic Regulator (LQR), is obtained from a full factorial design of experiments and refined through numerical optimization to ensure precise navigation while minimizing propellant consumption. The method presented in this paper successfully results in a fully functioning preliminary version of the LuNaDrone guidance and control system.

Keywords: Drone, Lunar pits, LQR, Guidance, Trajectory tracking

1 INTRODUCTION

In recent years, the Moon has been the target of a growing number of space missions. In 2023 and early 2024 alone, several soft landings on the lunar surface have been attempted, including: Intuitive Machines 1 (Odysseus), Peregrine Mission 1 by Astrobotic, Smart Lander for Investigating Moon (SLIM) by JAXA, Chandrayaan-3 by ISRO, Luna 25 by Roscosmos, and Hakuto-R M1 by ispace. Although not all of these missions have been entirely successful, the sheer number of them demonstrates a renewed interest in exploring the Moon's surface. Furthermore, it is evident that these efforts are no longer exclusively supported by agencies (e.g. through NASA's Artemis program and ESA's Terrae Novae exploration program).

Contact author: Stefano Pescaglia[1]

[1]C.so Duca degli Abruzzi 24 – 10129 – Torino (TO)
E-mail: stefano.pescaglia@polito.it

Indeed, the increasing number of private companies committed to provide lunar access services (such as ispace, Astrobotic and
Intuitive Machines) is a clear manifestation of a gradual consolidation of the so-called *Lunar Economy*; although agency initiatives, such as NASA's Commercial Lunar Payload Services (CLPS), are still providing some support for the development of this new market.

It is in this context, characterised by a growing number of precursor robotic missions dedicated to deliver science and technology to the lunar surface, that the use of small vehicles with post-landing mobility capabilities begins to assume a critical role. The lunar hopper that will be the subject of this paper belongs precisely to this category. As a matter of fact, such vehicles, and in particular small flying robots, can lend themselves very well to a wide range of applications, from scouting sites of interest to last-mile delivery of small payloads.

A relevant example of this can be found in [1], where the use of small flying spacecrafts is proposed as the most effective way to explore lunar pits that may give access to lava tubes. The exploration of these sites constitutes one of the most challenging usage scenarios for the lunar hopper presented

in this paper (henceforth referred to as *LuNaDrone*, which stands for Lunar Nano Drone), and their features significantly influence the design of the Guidance Navigation and Control (GN&C) system. In this paper, after introducing the reference mission scenario, i.e. the exploration of a lunar pit, and presenting the LuNaDrone project, the preliminary design of the drone's guidance and control system will be discussed. In particular, the focus will be on how the guidance algorithm and the controller have been implemented for this specific application. Finally, the results of dedicated simulations carried out in the MATLAB & Simulink environment will be presented to discuss the validity of the proposed approaches.

2 REFERENCE USE-CASE SCENARIO: LUNAR PITS EXPLORATION MISSION

The importance of lunar pits is mainly related to the possibility that they may provide access to lunar lava tubes. Lava tubes are natural underground formation originating from basaltic lava flows. The classification of some lunar rills as collapsed lava tubes has been a topic of discussion since the early 1970s [2]-[5]. Starting in 2011, with the Chandrayaan-1 mission [6], and in the following years with the NASA's GRAIL [7] and JAXA's SELENE [8] missions, it was possible to gather further indications of the actual presence of subterranean lava tubes. With the measurements collected during these missions and the subsequent studies, it was also possible to estimate the size of these formations in tens of kilometres in length and over 1 km in width [9]. The strong interest in the exploration of these sites stems from the strategic role they would play for future human settlements, as they provide shelter from energetic particles and cosmic radiation, micrometeoroids, and impact crater ejecta [10]. Furthermore, unlike the lunar surface, where temperature fluctuates between scorching daytime highs and very cold nighttime lows, the interior of a lava tube is expected to maintain a relatively constant temperature of about 20° C [11], which is of particular interest for robotic and human activities as, among other things, it would greatly reduce the mass and complexity of thermal control systems. Finally, these sites also hold a strong scientific significance as their exploration would provide better insights into the origin and formation of the Moon [12], [13].

The most relevant aspect for the purpose of this work is related to the accessibility conditions of these lunar lava tubes. The exploration of these tubes can be achieved only through roof openings known as skylights. In 2009, a lunar pit of more than 60 metres in diameter located in the Marius Hills was the first to be recognized as a possible skylight [14]. In 2010, two new possible skylights were found in Mare Tranquillitatis and Mare Ingenii [15]. Subsequent observations revealed that the pit located in the Marius Hills and the one located in Mare Tranquillitatis present tens of meters of floor extending beneath the ceiling, suggesting the presence of a subterranean void [12]. In the recent years, approximately 300 pits have been identified [1], a few of which presenting features that suggest the presence of underlying caves, particularly those situated in lunar maria. Nevertheless, without a direct exploration of these sites it is impossible to assess whether these voids actually extend further into a lava tube or not. The almost vertical walls of these access shafts consist of stacked lava flows, interleaved with paleo-regolith layers and more or less welded pyroclastic deposits. It is therefore clear that a rover exploration of such pits is not feasible, as any activity along the funnel would create mechanical instabilities, possibly resulting in dust avalanches and rockfalls [16]. Thus, other ways of exploration need to be conceived. In literature, different strategies have been considered for the exploration of potential skylights [13], [16] - [19]. An extensive comparison between these strategies and the proposal that is the subject of this paper, which employs LuNaDrone to fly inside these pits, was provided in [20].

3 LUNAR NANO DRONE – LuNaDrone

The LuNaDrone concept was first investigated in 2020 in a research project at the Department of Mechanical and Aerospace Engineering of Politecnico di Torino. Two years later, it led to the foundation of a spin-off, Evolunar s.r.l., which is currently engaged in the designed and development of the drone. Previous work has extensively presented both the lunar pit exploration mission concept and the LuNaDrone architecture [21] - [23]. Some of these aspects are also reported in this chapter to provide context for the following sections.LuNaDrone is a small spacecraft capable of flying over the lunar surface thanks to its own rocket propulsion system and its autonomous navigation system. Its small size (approx. 15 kg) is intended to make it compatible with even the smallest lunar landers, including those of private companies mentioned in the introduction chapter. The extreme mobilities capabilities of this vehicle allow a wide range of applications, from exploring sites of interest to last-mile delivery of small payloads. For example, LuNaDrone can perform scouting flights to identify resources to be mined and collect critical data for efficient mission planning by identifying potential hazards and locating the most promising sites, ensuring maximisation of commercial and scientific returns from future missions. Thanks to the ability to fly close to the lunar surface, LuNaDrone can collect measurements at a higher resolution than what would be achievable by orbiters and can fly over rough terrain that would otherwise be inaccessible to rovers. As a matter of fact, small rovers are not only limited by the geometry of the terrain, but also by the total distance they can cover during the mission, since they move only a few meters or centimetres per hour and are generally not designed to survive beyond the lunar day. Instead, by flying, LuNaDrone can reach the location required by the payload, which can be kilometres away from the lander, in a matter of minutes.

3.1 CONCEPT OF OPERATIONS

As mentioned above, of all these possible applications, the one that will be considered for the preliminary design of the guidance and control system is the exploration of lunar pits. This choice is motivated by the fact that this mission is

arguably the most demanding in terms of system requirements, as can be easily deduced by considering, for example, the very high position accuracy needed to avoid colliding with the pit walls during the flight. Considering this mission scenario, LuNaDrone needs to be deployed by the lander within a certain distance of the pit to be explored. If the lander employs terrain-relative navigation, it may be feasible to achieve pinpoint landings within 100 meters of the target, as demonstrated by the SLIM mission, where the Japanese spacecraft was able to land approximately 55 m east of the original target landing site [24]. However, in order to ensure suitability for a range of mission scenarios and different lunar landers (not all of which could be equipped with these navigation capabilities), a maximum distance of a few kilometres between the deployment site and the lunar pit has been considered. Please note that this should not be interpreted as the maximum distance that the drone is capable of covering, as this figure needs to take into account also the propellant-consuming manoeuvres that LuNaDrone shall perform to properly explore the interior of the pit. In fact, without these constraints on the flight profile, the same spacecraft configuration would be able to cover distances of one higher order.

Before separation from the lander, the mission's flight profile is updated to consider the true position and attitude of LuNaDrone. There are two possible strategies for detachment: the drone can either be placed on the lunar surface (e.g. by a robotic arm) or it can take off directly from the lander for example by using a rail attached to the side of the lander as a launch pad. After take-off, LuNaDrone will execute a fixed altitude trajectory, the height of which is determined by taking into account several factors like the requirements of the payload, the topography of the terrain, the performance of the GN&C system and the propellant consumption. Once the drone has reached the potential skylight, it will start a slow descent into the pit during which it will be possible to acquire scientific data of the surrounding walls. Then, the drone will hover at a safe height above the pit floor in order to minimise hazardous interactions between the surface and the thruster plumes. During this critical manoeuvre LuNaDrone will collect measurements of the inside environment of the pit that will be later used to determine the presence of a lava tube. After completing this critical phase, the drone will fly out of the pit and reach a preselected landing site that would allow communications between the drone and the lander. Once landed, LuNaDrone will transmit the scientific data collected during the flight to the lander, which will then relay this data back to Earth. Once communications have been completed, the drone will perform another flight (if possible), otherwise it will end its mission (at the current stage, the drone is not expected to survive the lunar night).

4 GN&C SYSTEM OVERVIEW

The diagram shown in Figure 1 summarises the main elements of the LuNaDrone's GN&C system. The "Navigation Algorithm" and "Navigation Sensors" blocks together constitute the Navigation system, which has already been presented in [21], [23] and will not be addressed in this paper, as a detailed knowledge of the Navigation system is not required for the preliminary design of the Control system. Indeed, according to the separation principle, if certain conditions hold, the problems of optimal control and state estimation can be decoupled. With regard to the work presented in this paper, it was therefore assumed that the output of the Navigation system (state estimation) corresponds exactly to the actual state (Plant output). As can be easily deduced from the diagram in Figure 1, this first implementation proposes an open-loop guidance. A closed-loop approach will be evaluated in subsequent versions. The actuators are represented by the "Main Thruster" and "Attitude Thrusters" blocks. While the controller outputs unbounded commands, the maximum force is actually limited by the maximum thrust that the rocket engines can exert. The same applies to the maximum torque, which is also affected by the relative position of the thrusters with respect to the drone's centre of mass.

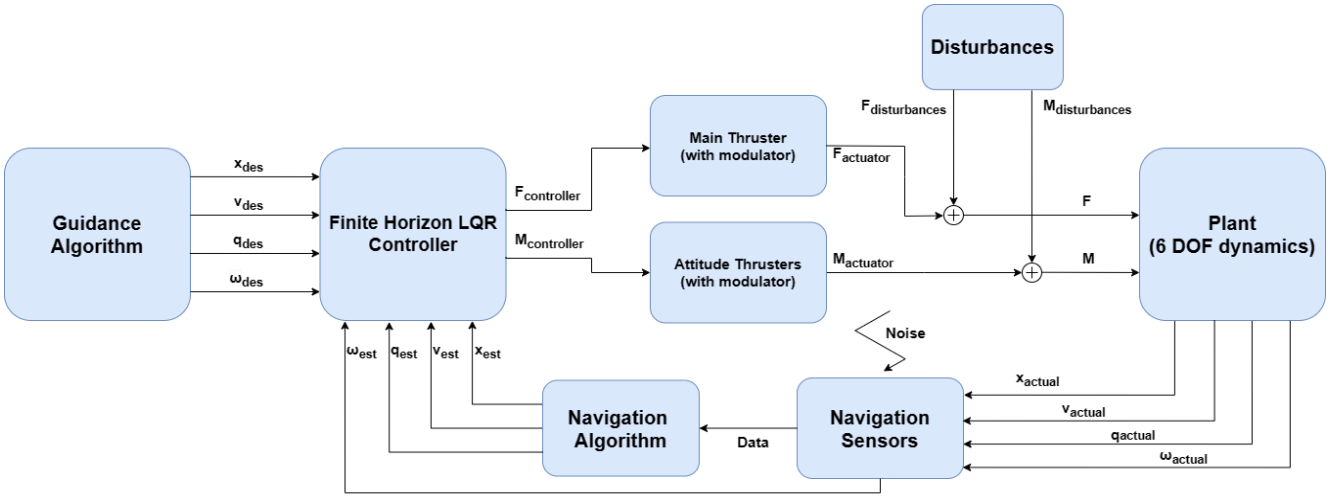

Figure 1 LuNaDrone's GN&C system diagram

The thrusters considered for LuNaDrone are equipped with solenoid flow control valves and the propellant feeding system is pressure fed. As a result, both the main engine and the Attitude Control System (ACS) thrusters can only deliver a single nominal value of thrust. To achieve lower time-average values, it is therefore necessary to operate the thrusters in pulsed mode. A Pulse-Width/Pulse-Frequency (PWPF) modulator has been selected to modulate the input signal of the ACS thrusters. This modulator has been implemented in several communication satellites and has been examined for different space applications as it offers several advantages such as low sensitivity to perturbations, high degree of freedom in adjusting, and reduced propellant consumption [25]. The modulator parameters have been properly set to take into account the switching constraints of LuNaDrone's thrusters, such as their minimum pulse time (t_{on}) and minimum time between pulses (t_{off}). For the main thrusters, a customised modulator was initially developed to vary both the amplitude and frequency of the command, which was eventually replaced by the modulator proposed in [26].

The forces and torques coming out of the thrusters' blocks do not perfectly match those entering the Plant because of disturbances. These disturbances include both physical phenomena, such as the forces resulting from propellant sloshing, as well as fictitious disturbances that serve to simulate the effect of the drone's centre-of-mass shifts, thrusters misalignments, deviations between the thrusters' true actuation profile and the ideal step profile, etc. In this first iteration, only thruster misalignments were properly modelled, while a white noise was added to account for the other effects. Although this may not lead to fully significant results (e.g. the propellant consumption obtained from these simulations could be either overestimated or underestimated), the introduction of white noise in the disturbances allowed the robustness of the control algorithm to be tested, which is of fundamental importance for this application.

5 GUIDANCE

The guidance algorithm has been the first to be developed as it served also as a preliminary tool for estimating propellant consumption. The LuNaDrone's flight-control concept of operations is similar to the one implemented for NASA's Mars Helicopter Ingenuity [27]. In the case of the lunar pit exploration mission, LuNaDrone will follow a fixed altitude trajectory that can be subdivided into a succession of elementary manoeuvres such as: vertical ascent, horizontal translation, vertical descent, and hovering (see Figure 2). The most critical manoeuvres involve take-off and landing, which deserve a separate in-depth discussion. For this preliminary analysis, these segments will be included in the vertical ascent and vertical descent manoeuvres.

5.1 VERTICAL ASCENT

The height of the fixed altitude trajectory that LuNaDrone should follow is set by mission control engineers and should take into account several factors like the topography of the terrain, the payload and GN&C system requirements, the propellant consumption, etc. Based on these considerations, the optimal distance from the lunar surface is expected to be a few tens of metres. For every elementary manoeuvre, the goal is to minimise propellant consumption while satisfying constraints and boundary conditions. The latter impose zero residual velocity at the start and end of each manoeuvre. Other constraints are related to the maximum velocity LuNaDrone is allowed to reach during the flight. In the case of vertical ascent and descent manoeuvres, the vertical velocity may be limited both for technical and scientific purposes. Taking these factors into account, we can easily derive the ideal thrust program that minimise gravity and misalignment losses. The optimal thrust program for the vertical ascent manoeuvre requires the main engine to exert the maximum continuous thrust it can deliver until the spacecraft reaches the right height and velocity to initiate a gravitational braking (during which the engine is cut off) so that the drone reaches the selected height with zero residual velocity. If the maximum allowable velocity (set by mission control engineers) is reached during the manoeuvre, the main engine will exert a thrust equal to the weight of the drone (which varies over time due to propellant consumption) until the start of the gravitational braking phase. This thrust program is simple enough to allow an analytical formulation of this manoeuvre, which is reported in Eq. 1.

$$\begin{cases} h = \frac{c^2}{g}\left\{\frac{\varphi_a}{T^*}\frac{m_i}{m_{wet}} + \frac{1}{2}\ln^2\left(\frac{1}{1-\varphi_a}\right) - \frac{1}{T^*}\frac{m_i}{m_{wet}}\ln\left(\frac{1}{1-\varphi_a}\right) + \right. \\ \qquad \left. + \ln\left(1-\frac{\varphi_{cs}}{1-\varphi_a}\right)\left[\frac{\varphi_a}{T^*}\frac{m_i}{m_{wet}} - \ln\left(\frac{1}{1-\varphi_a}\right)\right]\right\} \\ \square \\ V_{lim} = c\left[\ln\left(\frac{1}{1-\varphi_a}\right) - \frac{\varphi_a}{T^*}\frac{m_i}{m_{wet}}\right] \end{cases} \quad (1)$$

Where:

- h is the change in altitude.
- c is the effective exhaust velocity of the main engine, which is assumed to remain constant during the flight.
- g is the Moon's gravitational acceleration and is assumed to be homogeneous in space.
- m_{wet}, m_i are the drone's wet mass and the mass at the start of the manoeuvre respectively (which may differ from each other when previous manoeuvres have been performed).
- $T^* = T/(m_{wet}g)$, where T is the maximum continuous thrust (expressed in Newtons), which is assumed to remain constant during the manoeuvre.
- V_{lim} is the maximum vertical velocity that the drone could reach, given: h, T^*, I_{sp}, and m_i/m_{wet}.
- φ_a is the ratio between the propellant mass consumed during the acceleration phase (when the drone's velocity goes from zero to the minimum value between V_{max} and V_{lim}, where V_{max} is the maximum velocity set as an external constraint) and the initial mass m_i.
- φ_{cs} is the ratio between the propellant mass consumed during the constant speed phase (if present) and the initial mass m_i. The constant speed phase corresponds to the

phase when the main engine exerts a thrust equal to the weight of the drone, maintaining a vertical velocity equal to V_{max}.

The equations for this manoeuvre have been derived starting from the one reported in [28], which have been adapted for this specific application. The same equations can be expressed with the variables written as functions of time, allowing the guidance algorithm to provide the desired state and open-loop control action at each time instant.

5.2 VERTICAL DESCENT

The vertical descent is quite similar to the ascent manoeuvre. In Figure 2, the most relevant vertical descent is the one that allow the drone to enter the lunar pit. In this occasion the velocity is limited to allow the proper acquisition of scientific measurements of the exposed pit walls. The optimal thrust program that minimises gravity and misalignment losses is the following: (1) main engine off until V_{max} is reached, (2) constant speed phase (thrust equal to the weight of the spacecraft), (3) braking phase (maximum continuous thrust exerted by the engine until LuNaDrone comes to a complete stop. The equations describing these manoeuvres are similar to the one obtained for the vertical ascent:

$$\begin{cases} h = \frac{c^2}{g}\left\{-\frac{1}{2}\ln^2\left(1-\frac{\varphi_a}{1-\varphi_{cs}}\right) - \ln(1-\varphi_{cs})\left[\frac{\varphi_a}{T^*}\frac{m_i}{m_{wet}} + \right.\right. \\ \quad + \ln\left(1-\frac{\varphi_a}{1-\varphi_{cs}}\right)\Big] + \frac{1}{T^*}\frac{m_i}{m_{wet}}[\varphi_a + \\ \quad \left.\left. -(\varphi_a+\varphi_{cs}-1)\ln\left(1-\frac{\varphi_a}{1-\varphi_{cs}}\right)\right]\right\} \\ \\ V_{lim} = c\left[\frac{\varphi_a}{T^*}\frac{m_i}{m_{wet}} + \ln\left(1-\frac{\varphi_a}{1-\varphi_{cs}}\right)\right] \end{cases} \quad (2)$$

where φ_a in this case represent the ratio between the propellant consumed during the braking phase and m_i. Please also note that in this case both h and V_{lim} assume negative values.

5.3 HOVERING

The hovering manoeuvre enables LuNaDrone to maintain its position in space. Such a manoeuvre requires the propulsion system to exert enough thrust to cancel the weight of the spacecraft. Since LuNaDrone is not intended to land on the pit floor, this manoeuvre is critical to keep the spacecraft at a safe height above the ground (avoiding hazardous thruster plume interactions with the surface) while measurements of the interior surroundings are collected. The equation describing this manoeuvre is derived directly from the Tsiolkovsky rocket equation:

$$\varphi_h = 1 - e^{-\frac{g}{c}t_h} \quad (3)$$

Where t_h is the time duration of the manoeuvre and φ_H is the ratio between the propellant mass consumed and m_i.

5.4 HORIZONTAL TRANSLATION

During the horizontal translation manoeuvre, in order to maintain a constant altitude, the propulsion system has to provide a vertical component of the thrust that is equal to the LuNaDrone's weight, which changes over time due to propellant consumption. To move laterally, the propulsion system must provide a lateral thrust component. These lateral forces are obtained by tilting the axis of the thrust generated by the main engine. In fact, this approach leads to a lighter and more compact propulsion system as it doesn't necessitate the installation of dedicated thrusters for producing the lateral forces.Furthermore, even without taking into account the additional weight, the installation of lateral thrusters would still result in higher propellant consumption (assuming they have the same specific impulse as the main engine). Since thrust vectoring control (TVC) techniques are challenging to implement in this particular application, the orientation of the thrust axis is changed by tilting the entire spacecraft with the use of small ACS thrusters.

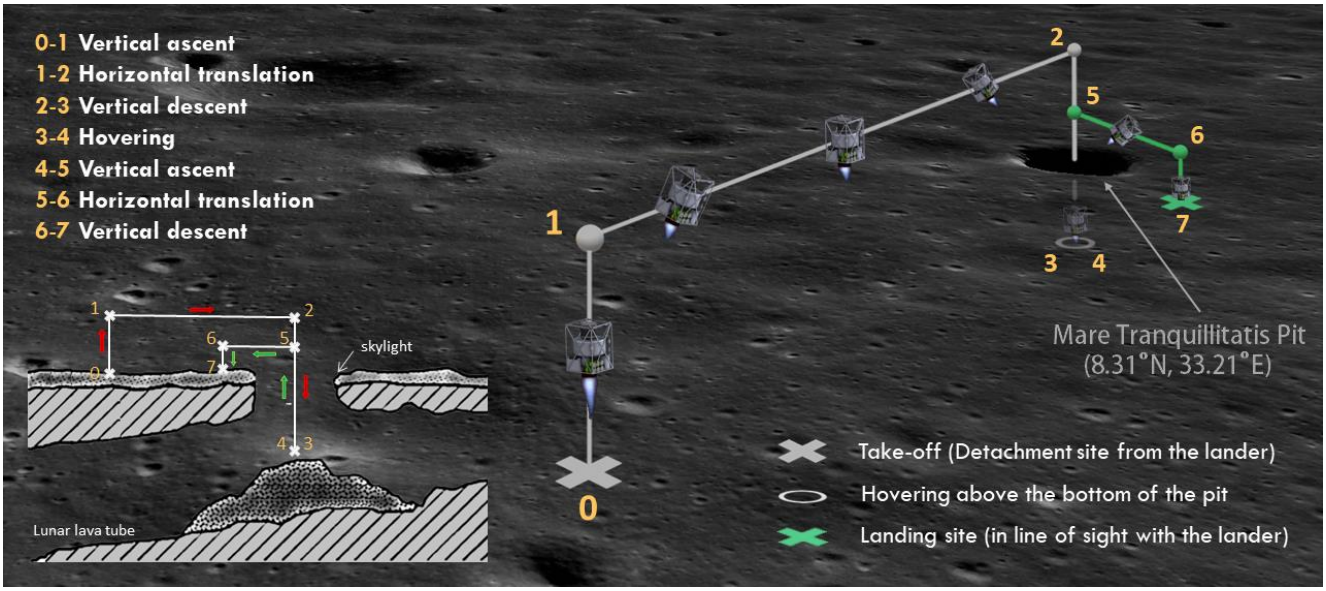

Figure 2 Diagram of an exploratory flight of the Mare Tranquillitatis Pit

With the introduction of a number of simplifying assumptions, such as considering only constant lateral accelerations, it was possible to derive an analytical formulation for this manoeuvre. This approach made it possible to quickly obtain preliminary estimates of propellant consumption and allowed the identification of important parameters for the GN&C design, such as the optimum maximum lateral velocity. However, assuming that the drone executes the acceleration and braking phases at constant acceleration values introduces discontinuities in the drone's attitude time history, which in turn leads to the definition of an unfeasible trajectory. To ensure continuity of the drone's attitude, both during the horizontal translation manoeuvre and between the end of the previous manoeuvre and the start of the next, it was decided to generate the optimum trajectory by constrained numerical optimisation. This also led to the identification of a thrust program that results in slightly less propellant consumption than what had been evaluated from the approximate solution.

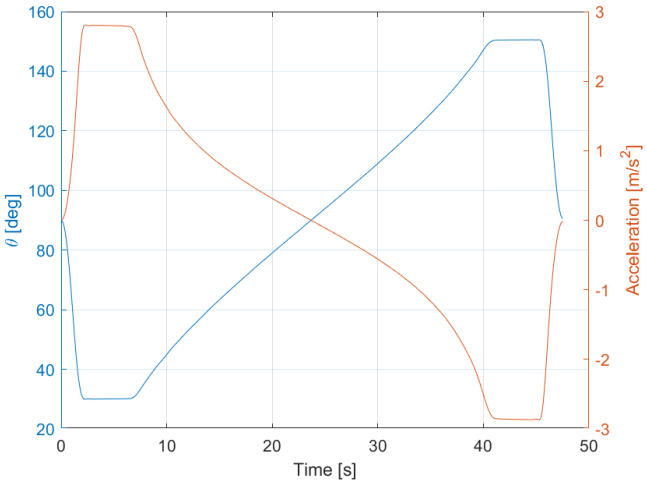

Figure 3 Pitch angle and lateral acceleration time history during a horizontal translation manoeuvre

Figure 3 reports the results of this optimisation. The lateral acceleration and the pitch angle of the drone are strictly dependent from each other, due to the fact that a non-zero value of the former can be achieved only by tilting the entire spacecraft. It is possible to express this simple relation by the following equation:

$$\theta = \operatorname{atan}\left(\frac{T_Z}{T_X}\right) = \operatorname{atan}\left(\frac{m(t)g}{m(t)a_X}\right) = \operatorname{atan}\left(\frac{g}{a_X}\right) \tag{4}$$

Where θ represents the pitch angle between the longitudinal body axis and the local horizon; a_X is the lateral acceleration; T_Z and T_X are the vertical and lateral thrust components, measured with respect to the inertial reference frame (is the guidance assumes that the thrust T is perfectly aligned with the longitudinal body axis of the drone). The optimal solution, in terms of propellant consumption, would exert the maximum lateral acceleration at the start and the end of the manoeuvre. In this case the pitch angle has been limited to a minimum of 30° and this is why the curve in Figure 3 saturates at this value. This limit was introduced to take into account the fact that the maximum continuous thrust of the main engine multiplied by the sine of the pitch angle must be equal to or greater than the weight of the drone.

5.5 GUIDANCE'S STATE AND CONTROL VECTORS

By assembling all these elementary flight segments together, it was possible to develop a guidance algorithm that was able to provide the time evolution of the following state and control vectors:

$$\boldsymbol{x_{des}} = \begin{bmatrix} X \\ Y \\ Z \\ v_X \\ v_Y \\ v_Z \\ q_0 \\ q_1 \\ q_2 \\ q_3 \\ \omega_x \\ \omega_y \\ \omega_z \end{bmatrix}, \quad \boldsymbol{u} = \begin{bmatrix} T \\ M_x \\ M_y \\ M_z \end{bmatrix} \tag{5}$$

Where the first six components of $\boldsymbol{x_{des}}$ represents the position and velocity of the spacecraft with respect the inertial reference frame, the next four elements are the scalar component (q_0) and the vector part of the quaternion describing the drone's attitude (the rotation from the inertial reference frame to the body-fixed reference frame), and the last three are the angular velocities measured with respect to the drone's body-fixed reference frame. The control terms of $\boldsymbol{u}$ are the thrust exerted by the main engine, which are ideally aligned with the z-axis of the body reference frame, and the torque components exerted by the ACS thrusters, which are measured with respect to the body-fixed reference frame.

6 CONTROLLER

LuNaDrone can be considered a multiple-input, multiple-output (MIMO) system, as its dynamics are influenced by one force (the main engine thrust) and three torques (see $\boldsymbol{u}$ in Eq. 5) and the output observed by the control system is a state vector with multiple components. The system is non-linear due to the nature of the equations that describe the drone's dynamics, and it is also time-variant because the LuNaDrone's mass and inertia moments vary during the flight due to propellant consumption. A Finite-Horizon Linear Quadratic Regulator (LQR) was chosen as the controller due to its suitability for MIMO systems, and its ability to control both attitude and position with a single control loop. In this case, it is also relatively easy to implement, since the equations of dynamics are known, as is the trajectory against which they are to be linearised. Indeed, LQR is one of the most powerful controllers for trajectory tracking in modern control theory [29] - [31]. The linearized system of the LQR, however, shows much higher time

dependence than the simple variation of mass properties of the non-linear system, due to the fact that the linearization point changes with time as the drone flies along the trajectory, resulting in time-varying state and control terms appearing in the state and input matrices of the linear system. LQR was preferred to Sliding Mode Control (SMC), as the latter would possibly have required the implementation of multiple control loops and because defining its sliding surface would have been non-trivial for this application. In this application, an integral action has been added (LQRI) as proposed in [32], in order to reduce the residual error caused by unmodelled dynamics. Finally, the finite horizon formulation was implemented, as the infinite horizon version of LQR is not suitable for tracking problems in time-variant systems. An in-depth description of this method can be found in [29]. In this formulation the gain matrix K for LQR is calculated from the solution of the differential Riccati equation (DRE) at each time instant. The DRE is integrated backwards in time, starting from the solution of the algebraic Riccati equation (ARE) evaluated at the final point of the trajectory.

In the LuNaDrone's case, the augmented error state including integral actions is equal to:

$$\boldsymbol{\delta\tilde{x}} = \begin{bmatrix} \boldsymbol{\delta x} \\ \int_0^t (X - X_{des})dt \\ \int_0^t (Y - Y_{des})dt \\ \int_0^t (Z - Z_{des})dt \\ \int_0^t (q_{e_3})dt \end{bmatrix}, \qquad \boldsymbol{\delta x} = \begin{bmatrix} X - X_{des} \\ Y - Y_{des} \\ Z - Z_{des} \\ v_X - v_{X\,des} \\ v_Y - v_{Y\,des} \\ v_Z - v_{Z\,des} \\ \delta q_1 \\ \delta q_2 \\ \delta q_3 \\ \omega_x - \omega_{x\,des} \\ \omega_y - \omega_{y\,des} \\ \omega_z - \omega_{z\,des} \end{bmatrix} \tag{6}$$

Unlike the state vector x_{des} provided by the guidance algorithm, the error state vector does not include the quaternion's scalar component as the small-angle approximation can be applied, meaning that $\delta q_0 \cong 1$ and only the vector part is considered. This also inherently eliminates the extra degree of freedom of the quaternion in describing a 3D rotation, which would create an uncontrollable system. As can be seen from Eq. 6, not all 12 integral errors have been considered, but only those related to position and rotation around the drone's longitudinal axis. The latter is described as the integral error of the last component of the quaternion's vector part. Indeed, in a neighbourhood sufficiently close to the identity, the vector components behave similarly to a Euler angle representation of the rotation, scaled by half [33]. The reason why only 4 integral errors were considered, instead of all 12, comes from controllability considerations. A system is said to be controllable at time t_0 if it is possible by means of an unconstrained control vector to transfer the system from any initial state $x(t_0)$ to any other state in a finite interval of time [34]. While fully knowing that a proper controllability analysis would need to take into account the non-linear and time-variant nature of the system, to get a first indication of the controllability it was decided to consider the formulation for linear time-invariant systems, evaluating the rank of the controllability matrix [35] at each point of the trajectory individually. The analysis conducted on the complete augmented state vector (which comprises 24 elements) showed that the controllability matrix has always rank 16, except for the points where the main engine is switched off, in which case the rank drops to 12. This decrease in rank is a direct result of the linearisation, as one of the effects of linearising at these points, where the thrust is zero, is that the system is no longer able to consider the possibility of switching on the main engine to properly control the drone (which is instead embedded in the actual non-linear time-variant system). To ensure system controllability it is necessary to exclude 8 elements of the complete augmented state vector. To identify which elements are to be excluded, a few considerations can be made. The most relevant is arguably the fact that since the drone has to tilt in order to move laterally, residual errors on both position and attitude can not be cancelled simultaneously. It was therefore decided to reduce the augmented state vector to 16 elements, choosing to include only the integral actions shown in Eq. 6. Indeed, the controllability matrix of the system with 16 states and engine on is full rank and the positive results obtained in the following simulation have proved the validity of this choice.

6.1 OPTIMISATION AND TUNING

In order to find the optimal parameters of the controller, a Simulink model of the LuNaDrone's system has been developed. This model, reported in Figure 4, essentially implements the diagram in Figure 1. The total number of parameters is 29, where 9 are related to the three PWPF modulators (one per body axis), 16 are the diagonal entries of the state-cost weighted matrix Q of the LQR, and 4 are to the diagonal entries of the input-cost weighted matrix R. As a first step, a full factorial design of experiments (DoE) was performed, in which only 10 independent parameters were considered, according to the following criteria:

- Each PWPF modulator for the torques (one per each body axis) has the same three parameters.
- Five independent parameters were set for the Q matrix, one for the three error-state elements concerning position, one for the three velocity error components, one for the three angular velocity error components, one for the vector part of the quaternion error and one for the four integral errors.
- Two independent parameters were set for the R matrix, one related to the main engine thrust control term and one for the three torque control terms of the ACS thrusters.

For the sake of simplicity, the optimization problem has been set up with a cost function in which only propellant consumption is taken into account, while compliance with the guidance's trajectory is introduced by defining a set of non-linear constraints on the position of the drone (which

should never deviate more than 2 metres from the guidance's trajectory).

The 20 best DoE results were selected and used as starting points in a gradient descent optimisation algorithm. In this case, there were 20 independent parameters, selected according to the following criteria:

- Six parameters related to the PWPF modulators. Each modulator has three independent parameters, but it was decided to use the same parameters for the two modulators concerning the actuation torques around the x- and y-body-axes.
- Eleven parameters related to the matrix Q. Again, it was decided to assign the same parameter to the x and y components of the same physical quantity (position, velocity, angular velocity, etc.).
- Three parameters related to R, one for the main engine thrust, one for the torque around the z body axis, and the same parameter for both the body x- and y-axes.

The rationale behind these criteria comes from the symmetry of the drone along two perpendicular planes intersecting on the z-axis and the design goal of obtaining a set of optimization parameters that are independent from the specific direction of the trajectory taken into consideration (i.e. the drone should be able to perform the same trajectory by tilting forward any of its 4 lateral sides).

7 CONCLUSIONS

In this paper the method used for the preliminary design of the LuNaDrone's guidance and control system has been presented. After introducing the LuNaDrone project and its most demanding use-case, i.e. the exploration of a lunar pit, an overview of the drone's GN&C system was provided. Next, the guidance algorithm was introduced together with the individual elementary manoeuvres that constitute the flight profile. The guidance algorithm thus developed has been able to provide the time evolution of the desired state and controls vectors. Finally, the preliminary design of the control system has been discussed, with particular focus on the optimisation of the selected algorithm, which is based on a LQR Finite Horizon controller. In order to tune the parameters of the controller, a full factorial DoE has been performed, followed by numerical optimization for further refinement. The obtained results are promising: even with strong white-noise disturbances, the control system is able to keep LuNaDrone on track (it does not deviate more than half a metre from the ideal trajectory), while maintaining low propellant consumption. The method presented in this paper has successfully led to a fully functioning preliminary version of the LuNaDrone's guidance and control system. Future works will involve the development of closed-loop guidance algorithms for real time trajectory calculation, in-depth analysis of stability and controllability and enhanced optimization methods for parameter tuning. Future works will also explore leveraging FBGs as both motion and thermal sensors to enhance redundancy and increase the LuNaDrone's ACS performance. In fact, as presented in [36], [37], [38], these sensors would be able to detect rapid temperature changes, making it possible to distinguish between the sunlit and shaded faces of the drone, thus providing additional information for navigation. In addition, there is much evidence demonstrating the survival of FBGs in the space environment [37].

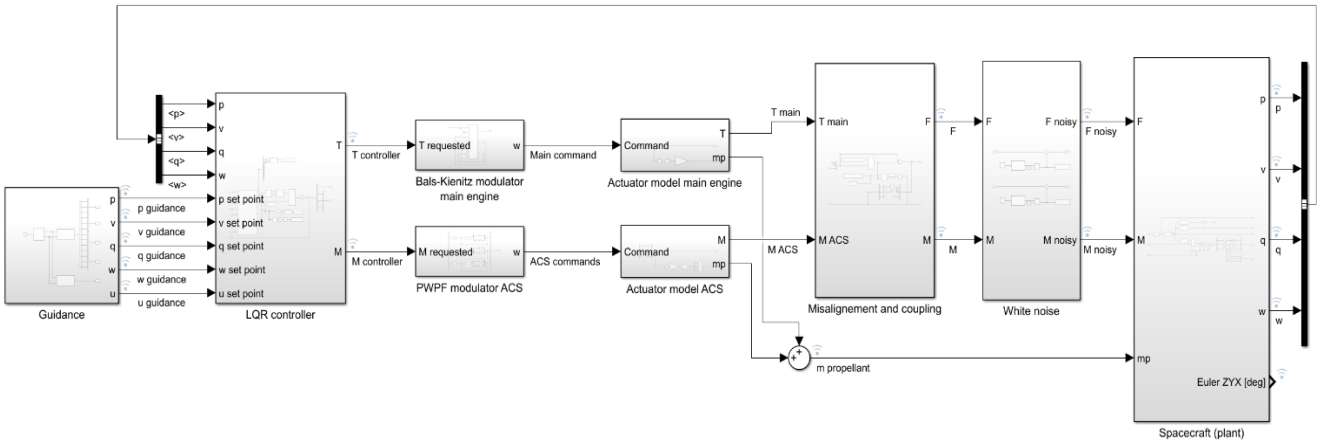

Figure 4 LuNaDrone's Guidance and Control System Simulink model

REFERENCES

[1] R. V Wagner and M. S. Robinson, Lunar Pit Morphology: Implications for Exploration. *J Geophys Res Planets*, Vol. 127.

[2] V. R. Oberbeck, W. L. Quaide, and R. Greeley, On the Origin of Lunar Sinuous Rilles. *Modern Geology*, Vol. 1, pp. 75-80, 1969.

[3] R. Greeley, Lava tubes and channels in the lunar Marius Hills. *The Moon*, Vol. 3, pp. 289-314, 1971.

[4] F. Horz, Lava tubes - Potential shelters for habitats. *Lunar Bases and Space Activities of the 21st Century*, W. W. Mendell, Ed., 1985, pp. 405-412.

[5] C. R. Coombs and B. R. Hawke, A Search for Intact Lava Tubes on the Moon: Possible Lunar Base Habitats. *Lunar Bases and Space Activities of the 21st Century*, Sep. 1992, p. 219.

[6] A. S. Arya, R. P. Rajasekhar, G. Thangjam, Ajai, and A. S. K. Kumar. Detection of potential site for future human habitability on the Moon using Chandrayaan-1 data. *Curr Sci*, Vol. 100, No. 4, pp. 524-529, 2011.

[7] L. Chappaz et al, Evidence of large empty lava tubes on the Moon using GRAIL gravity. *Geophys Res Lett*, Vol. 44, No. 1, pp. 105-112, 2017.

[8] T. Kaku et al., Detection of Intact Lava Tubes at Marius Hills on the Moon by SELENE (Kaguya) Lunar Radar Sounder. *Geophys Res Lett*, Vol. 44, No. 20, pp. 10, 110-155, 161, 2017.

[9] D. M. Blair et al., The structural stability of lunar lava tubes. *Icarus*, Vol. 282, pp. 47-55, 2017.

[10] G. De Angelis, J. W. Wilson, M. S. Clowdsley, J. E. Nealy, D. H. Humes, and J. M. Clem, Lunar lava tube radiation safety analysis.. *J Radiat Res*, Vol. 43 Suppl, pp. 41-45, 2002.

[11] T. Horvath, P. O. Hayne, and D. A. Paige, Thermal and Illumination Environments of Lunar Pits and Caves: Models and Observations From the Diviner Lunar Radiometer Experiment. *Geophys Res Lett*, Vol. 49, No. 14, 2022.

[12] M. S. Robinson et al., Confirmation of sublunarean voids and thin layering in mare deposits. *Planet Space Sci*, Vol. 69, No. 1, pp. 18-27, 2012.

[13] I. A. Nesnas, L. Kerber, A. Parness, R. Kornfeld, G. Sellar, and others, Moon Diver: A Discovery Mission Concept for Understanding the History of Secondary Crusts through the Exploration of a Lunar Mare Pit., *2019 IEEE Aerospace Conference*, pp. 1-23,2019.

[14] J. Haruyama et al., Possible lunar lava tube skylight observed by SELENE cameras. *Geophys Res Lett*, Vol. 36, No. 21, pp. 7-8, 2009.

[15] J. Haruyama et al., *New Discoveries of Lunar Holes in Mare Tranquillitatis and Mare Ingenii*, 2010.

[16] P. F. Miaja et al., RoboCrane: A system for providing a power and a communication link between lunar surface and lunar caves for exploring robots. *Acta Astronaut*, Vol. 192, pp. 30-46, 2022.

[17] W. Whittaker, *Technologies Enabling Exploration of Skylights, Lava Tubes and Caves*, 2012.

[18] W. Whittaker, U. Wong, and S. Huber, *Exploration of Planetary Skylights and Tunnels*, 2014.

[19] R. Tonasso et al., A lunar reconnaissance drone for cooperative exploration and high-resolution mapping of extreme locations'. *Acta Astronaut*, Vol. 218, pp. 1-17, 2024.

[20] S. Pescaglia, G. Bortolato, P. Maggiore, and P. Messidoro, LuNaDrone: Small Autonomous Spacecraft for Lunar Lava Tubes Exploration. *Proc. Of 2022 IEEE 9th International Workshop on Metrology for AeroSpace, MetroAeroSpace*, 2022.

[21] S. Pescaglia, G. Bortolato, P. Maggiore, P. Messidoro, and R. Vittori, LuNaDrone: nano drone for Lunar Exploration. *Proc. of IAC-22,A3,IP,61,x71889*, IAF, 2022.

[22] S. Pescaglia, R. Barbieri, G. Bortolato, P. Maggiore, P. Messidoro, and R. Vittori, Analysis of the Thermal Environment in the LuNaDrone Exploration Mission of Lunar Lava Tubes. *Proc. of 2023 IEEE 10th International Workshop on Metrology for AeroSpace, MetroAeroSpace*, 2023.

[23] S. Pescaglia, G. Bortolato, P. Maggiore, P. Messidoro, and R. Vittori, LuNaDrone: a small flying vehicle for lunar pit exploration. *Proc. of 74 th International Astronautical Congress (IAC)*, 2023.

[24] Jaxa., *Outcome for the Smart Lander for Investigating Moon (SLIM) 's Moon Landing*, 2024.

[25] A. Khosravi and P. Sarhadi, Tuning of Pulse-Width Pulse-Frequency Modulator using PSO: An Engineering Approach to Spacecraft Attitude Controller Design. *Automatika*, Vol. 57, 2016.

[26] J. Bals and K. H. Kienitz, *A comprehensive approach to pulse modulation for attitude control with thrusters subject to switching restrictions. I & II.*, 2005.

[27] H. F. Grip et al., Flight control system for nasa's mars helicopter. *Proc. of AIAA Scitech 2019 Forum*, American Institute of Aeronautics and Astronautics Inc, AIAA, 2019.

[28] J. W. Cornelisse, H. F. R. Schoyer, and K. F. Wakker, *Rocket propulsion and spaceflight dynamics*, London: Pitman, 1979.

[29] R. Tedrake, *Underactuated Robotics*, 2023.

[30] S. Venturini and E. Bonisoli, Design of a Spherical Pendulum Didactic Test Rig. *International Journal of Mechanics and Control*, Vol. 19, No. 01, pp. 69-76, 2018.

[31] M. R. Homaeinezhad, M. Youshi, A. Foroughimehr, and B. Rachidi, Designing Sliding Mode Observer for Estimation of Euler and Longitudinal-Lateral Flapping Angles in Hover Flight Motion of a Helicopter. *International Journal of Mechanics and Control*, Vol. 20, No. 02, pp. 77-89, 2019.

[32] H. G. Malkapure and M. Chidambaram, 'Comparison of Two Methods of Incorporating an Integral Action in Linear Quadratic Regulator. *IFAC Proceedings Volumes*, Vol. 47, No. 1, pp. 55-61, 2014.

[33] M. Farrell, J. Jackson, J. Nielsen, C. Bidstrup, and T. McLain, Error-State LQR Control of a Multirotor UAV. *Proc. of 2019 International Conference on Unmanned Aircraft Systems (ICUAS)*, 2019, pp. 704-711.

[34] Katsuhiko. Ogata, *Modern control engineering*, Prentice-Hall, 2010.

[35] C.-Tsong. Chen, *Linear system theory and design*, Oxford University Press, 1999.

[36] A. Aimasso, G. Charruaz, M. Bertone, C. Ferro, M. D. L. Dalla Vedova and P. Maggiore, Test bench and control logic development for dynamic thermal characterization of optical sensors. *International Journal of Mechanics and Control*, Vol. 24, No. 2, pp. 69-76, 2023.

[37] E. Brusa, M. D. Vedova, L. Giorio and P. Maggiore, Thermal condition monitoring of large smart bearing through fiber optic sensors. *Mechanics of Advanced Materials and Structures*, Vol. 28, No. 11, pp. 1187-1193, 2021.

[38] M. D. L. Dalla Vedova, P. C. Berri, P. Maggiore, and G. Quattrocchi, Design and development of innovative FBG-based fiber optic sensors for aerospace applications. *Journal of Physics: Conference Series*, Vol. 1589, No. 1, p. 012012, Jul. 2020.